NACA RM L52E06

NACA

RESEARCH MEMORANDUM

EFFECTS OF STABILIZING FINS AND A REAR-SUPPORT STING ON THE BASE PRESSURES OF A BODY OF REVOLUTION IN FREE FLIGHT AT MACH NUMBERS FROM 0.7 TO 1.3

By Roger G. Hart

Langley Aeronautical Laboratory
Langley Field, Va.

NATIONAL ADVISORY COMMITTEE
FOR AERONAUTICS

WASHINGTON

September 22, 1952
Declassified May 25, 1956

NATIONAL ADVISORY COMMITTEE FOR AERONAUTICS

RESEARCH MEMORANDUM

EFFECTS OF STABILIZING FINS AND A REAR-SUPPORT STING ON THE BASE PRESSURES OF A BODY OF REVOLUTION IN FREE FLIGHT AT MACH NUMBERS FROM 0.7 TO 1.3

By Roger G. Hart

SUMMARY

Ogive-cylindrical fuselages of fineness ratio 11 have been flight-tested with and without stabilizing fins. Base-pressure measurements over a range of free-stream Mach numbers from 0.7 to 1.3 indicated that the fins reduced the base drag. A rear-support sting similar to those used in wind tunnels was tested with one of the fuselages and found to reduce base suction by 40 percent at subsonic speeds, but to have little effect at Mach numbers above 1.15.

INTRODUCTION

One limitation of flight-testing techniques is that, in general, an aircraft component can be tested only as part of a combination which is aerodynamically and structurally capable of stable flight. Because of interference, it is necessary in some investigations to vary the parameters of several components in order to evaluate the effects of one. In other investigations, interference effects are small or can be made so by proper design of the test vehicles. In a few cases, it is feasible to fly isolated components. The results presented herein were obtained by that method.

In the present investigation three wingless, finless bodies were flight tested at the Langley Pilotless Aircraft Research Station at Wallops Island, Va. The fuselage chosen for these tests was an ogive-cylinder of fineness ratio 11 which had previously been used in free-flight investigations of base pressure, wing drag, and damping in roll (refs. 1 to 4, for examples). The models were boosted to supersonic speeds by external rockets, then allowed to coast freely. Stable flight was made

possible by a special construction which placed the center of gravity less than two body diameters aft of the nose tip. Drag and base pressure were measured for the isolated fuselages, and these values were then compared with previous data to obtain the drag of a fin configuration and its effect on base pressures. One of the models had a simulated wind-tunnel support sting, and its effects on base pressure were determined. The tests covered a range of Mach numbers from 0.7 to 1.3 and Reynolds numbers from 15×10^6 to 45×10^6.

SYMBOLS

c	atmospheric speed of sound, ft/sec
C_D	total-drag coefficient of a configuration (based on body frontal area)
C_{D_B}	base-drag coefficient (based on body frontal area)
C_{D_F}	fin-drag coefficient (based on exposed fin plan-form area)
l	body length, ft
M	Mach number, V/c
p	atmospheric pressure, lb/sq ft
p_B	base pressure, lb/sq ft
P_B	base-pressure coefficient, $\frac{p_B - p}{\frac{1}{2}\rho V^2}$
R	Reynolds number, $\rho V l/\mu$
V	air speed, ft/sec
ρ	atmospheric density, slugs/cu ft
μ	atmospheric viscosity, lb sec/sq ft

MODELS

The test configurations are shown in figures 1 to 4. All had the same fuselage shape – a body of revolution of fineness ratio 11 formed by joining a fineness-ratio-3.5 ogival nose to a cylinder. Coordinates of the nose portion are listed in table I. Configuration A consisted of this fuselage without modifications or appendages. The other test configurations had one or more of the following: a rear-support sting similar to those used in wind tunnels, a rocket tail nut, four stabilizing fins, and a pointed nose sting. Data for configurations E and C were originally presented in references 3 and 4, respectively. Data for the finless configurations and for configuration G are presented herein for the first time.

Configurations C, E, and G were stabilized by four fins spaced equally around the body. The leading edge of each fin was swept back 45°, and the plan form was tapered from a root chord of 8.38 inches to a tip chord of 1.38 inches. The exposed fin aspect ratio was 1.43. The fins measured 0.091 inch in thickness and were rectangular in section except for rounded leading edges.

The finless models depended for their stability on a special construction which placed the center of gravity at station 9.7 for configurations A and D and at station 0.25 for configuration F. The cylindrical part of the fuselage consisted of a thin balsa-wood shell reinforced by light plywood bulkheads. Mercury and lead ballast was used in the noses of configurations A and D, and a lead-weighted nose sting was used for configuration F. The sting was approximately five body diameters in length and had at its apex a cone of the same angle as the nose tip which it replaced.

The models were smooth and fair. Metal surfaces were polished, and wood surfaces were sanded and finished with clear lacquer. Plastic fillers were used to eliminate small indentations.

TESTS

The finless models were launched and accelerated to supersonic speeds by modified HVAR rocket motors. (See fig. 4.) Thrust was applied by means of a steel thrust tube, which extended from the nose of the booster through the lightly constructed cylindrical portion of the model and forward to heavier structural members in the nose. After burnout the booster, having a higher drag deceleration rate than the model, quickly separated. The thrust tube withdrew with the booster, and the model flew freely.

Configuration G employed a two-stage propulsion system. The first stage, or "booster," was an external HVAR rocket motor. The second stage, or "sustainer," was an internal 3.25-inch Mk 7 rocket motor. During the first part of the flight the booster engaged the sustainer by means of a nozzle plug adapter. Shortly after the booster stopped thrusting, the model and booster separated because of a difference in their drag deceleration rates. Then the sustainer motor fired, bringing the model to its maximum speed. The drag data were obtained during the period of coasting flight after sustainer burnout.

The models were tracked by Doppler radar velocimeter and SCR-584 radar theodolite to determine altitude, speed and direction of flight, and deceleration along the flight path. Atmospheric conditions were measured by means of radiosonde balloons released immediately after the flights. Drag was determined from the model deceleration rate after subtracting the proper component of gravity.

One of the finless models was instrumented for the telemetering of base pressures. By means of a two-channel telemeter, pressures on the rim of the base and inside the hollow body were transmitted continuously to a ground receiving station. Configurations B and A correspond to the base-pressure model before and after booster separation. For this flight the booster thrust tube was made to resemble a wind-tunnel rear-support sting.

The major sources of error in determining drag coefficients by the previously described technique are (1) inaccuracies in the instruments and in the reduction of instrument data, (2) inaccuracy in the manufacture of models, and (3) air currents, which cause errors in airspeed. Assuming that all of these tend to be of a random nature, the probable error can best be estimated by noting the discrepancies among faired curves for models of the same configuration. This has been done for a number of previously tested models of configuration E. On that basis, the probable error in drag coefficient has been estimated to be less than 4 percent for the present tests.

In reducing the present data, the air was assumed to be at rest relative to the ground. Therefore, any current motion which may have existed at the time of the flight tests has resulted in an airspeed error which is approximately equal to the velocity component of the current in the direction of the flight path. Since the aerodynamic coefficients are based on $\frac{1}{2}\rho V^2$, the percentage error in the coefficients due to currents is about twice that in V. The airspeed error which would be required to produce all of the observed scatter in C_D would be about ±20 feet per second. This value represents an upper limit for the probable error in airspeed. The true value is, according to other indications, closer to half that value. The probable error in Mach number is then about ±0.01.

The measurements of base pressure and of atmospheric pressure are accurate to about ±0.07 pound per square inch. These errors, together with a Mach number error of ±0.01, lead to maximum errors in base-pressure coefficient of ±0.030 at Mach number 0.8 and ±0.013 at Mach number 1.25.

By using the theory of reference 5, stability calculations were made for the finless body with the rearmost center-of-gravity location. The results indicated that the model would trim at an angle of attack of less than 1°. Although no angle-of-attack measurements were made for the models in flight, it is assumed here that the values which existed were, like the theoretical values, too small to have appreciable effects on drag or base pressure.

Total-drag coefficients for configurations A, D, E, F, and G, and base-drag coefficients for configurations A, B, and C are presented herein for the ranges of Mach numbers and Reynolds number shown in figure 5.

RESULTS AND DISCUSSION

Base-Pressure Data

As shown in figure 6, the rear-support sting reduced the absolute magnitude of the base-pressure coefficients by about 40 percent at subsonic speeds. With increasing Mach number the effect decreased rapidly, and, at Mach numbers above 1.15, the rear-support sting had no significant effect on base pressures.

Throughout the present test range the stabilizing fins had the effect of decreasing the base drag. This effect is shown in figures 7 and 8, where base-pressure data for configurations A and C are compared. In reference 6, other fin configurations located similarly on a cylindrical body were shown to increase base suction at supersonic speeds. This increase was attributed to the fin-pressure fields impinging on the "dead-air" region at the base of the body. Because of the rectangular section of the present fins, low pressures are confined to a small region just behind the blunt trailing edge. It is believed that, in the present case, the predominant effect is that of low-momentum air from the fin-body junctures being drawn into the region behind the body and relieving the base suction.

Drag Data

Drag data for the finless configurations A, D, and F are shown in figure 9 and the data for the fin-stabilized configurations E and G are shown in figure 10. Effects of the tail nut and nose sting are seen to

be small and within the test accuracy, though the data in both figures indicate that the nose sting increases the drag somewhat. An increment of 0.009 in C_D, which is of the same order as that noted, can be obtained by assuming a viscous drag coefficient of 0.0023 to act over the wetted cylindrical area of the sting. The data in figure 9 indicate that the nose sting also had the effect of lowering the force-break Mach number. Since this effect is far less pronounced in figure 10, it appears likely that some, if not all, of the shift is due to Mach number error.

Fin-drag coefficients are shown in figure 11. These have been obtained from the drag-coefficient increments between configurations D and E and between F and G, and they therefore include interference effects. Agreement is good except in the Mach number range from 0.9 to 1.0, where the apparent shifts in force-break Mach number had a large effect on the drag-coefficient increments. Included in this figure is a curve representing the change in base drag caused by adding fins to configuration A. The interference-drag values have been based on fin area for comparison here.

In figure 12, coefficients of fore drag (total drag minus base drag) for configuration A are compared with theoretical estimates of their components. Flight Mach numbers and body-length Reynolds numbers were used to calculate (by the method of ref. 7) the average viscous-drag coefficients for a wholly turbulent flat plate, and these were assumed to act over the wetted area of the forebody. Unpublished subsonic pressure distributions obtained in the Langley high-speed 7- by 10-foot tunnel indicate that the pressure drag on the nose is negligible at Mach numbers below 0.9. Thus, the fore drag consists almost entirely of viscous drag at these Mach numbers. The low level of the subsonic fore-drag coefficient indicates that laminar flow existed over a significant part of the body.

The supersonic pressure drag was estimated by the method of reference 8 and by the graphical method of reference 9. At Mach numbers from 1.1 to 1.25, the difference between estimated and measured fore-drag coefficients is nearly constant. A large part of this discrepancy may be due to the assumption of a wholly turbulent boundary layer on the body. In reference 10, pressure drag calculated for a body by the graphical method was found to be in good agreement with experiment at Mach numbers as low as 1.05. This result did not hold true in the present tests. The poor agreement shown at Mach number 1.05 may be due to the lower fineness ratio of the present nose.

CONCLUDING REMARKS

Isolated fuselages were flight-tested at Mach numbers from 0.7 to 1.3 in order to determine the contributions of the body and the fin-body interference to the total drag of previously tested combinations. A set of stabilizing fins of nearly rectangular section was found to decrease the body base drag over the Mach number range of the tests. One of the finless bodies had a rear-support sting similar to those used in wind tunnels. The sting reduced base suction by about 40 percent at subsonic speeds, but had no measurable effect at Mach numbers above 1.15.

It has been found that a simple nonspinning ogive-cylindrical body can be stabilized by internal ballasting. The present results also suggest that, where internal ballasting is inadequate because of boattailing or other body shape factors, a weighted nose sting can be used. Thus, the test techniques described herein may be applicable to many fuselages of practical interest.

Langley Aeronautical Laboratory
National Advisory Committee for Aeronautics
Langley Field, Va.

REFERENCES

1. Sandahl, Carl A., Bland, William M., Jr., and Strass, H. Kurt: Effects of Some Airfoil-Section Variations on Wing-Aileron Rolling Effectiveness and Drag As Determined in Free Flight at Transonic and Supersonic Speeds. NACA RM L9D12, 1949.

2. Pittel, Murray: Flight Tests at Supersonic Speeds to Determine the Effect of Taper on the Zero-Lift Drag of Sweptback Low-Aspect-Ratio Wings. NACA RM L50F30a, 1950.

3. Welsh, Clement J.: Results of Flight Tests to Determine the Zero-Lift Drag Characteristics of a 60° Delta Wing With NACA 65-006 Airfoil Section and Various Double-Wedge Sections at Mach Numbers From 0.7 to 1.6. NACA RM L50F01, 1950.

4. Peck, Robert F.: Flight Measurements of Base Pressure on Bodies of Revolution With and Without Simulated Rocket Chambers. NACA RM L50I28a, 1950.

5. Allen, H. Julian: Estimation of the Forces and Moments Acting on Inclined Bodies of Revolution of High Fineness Ratio. NACA RM A9I26, 1949.

6. Spahr, J. Richard, and Dickey, Robert R.: Effect of Tail Surfaces on the Base Drag of a Body of Revolution at Mach Numbers of 1.5 and 2.0. NACA TN 2360, 1951.

7. Van Driest, E. R.: The Turbulent Boundary Layer for Compressible Fluids on a Flat Plate With Heat Transfer. Rep. No. AL-997, North American Aviation, Inc., Jan. 27, 1950.

8. Von Kármán, Theodor, and Moore, Norton B.: Resistance of Slender Bodies Moving With Supersonic Velocities With Special Reference to Projectiles. Trans. A.S.M.E., vol. 54, no. 23, Dec. 15, 1932, pp. 303-310.

9. Thompson, Jim Rogers: A Rapid Graphical Method for Computing the Pressure Distribution at Supersonic Speeds on a Slender Arbitrary Body of Revolution. NACA TN 1768, 1949.

10. Thompson, Jim Rogers: Measurements of the Drag and Pressure Distribution on a Body of Revolution Throughout Transition From Subsonic to Supersonic Speeds. NACA RM L9J27, 1950.

TABLE I

BODY COORDINATES IN INCHES

Station	Radius
0	0
1.00	.25
2.00	.48
3.00	.71
4.25	.99
5.00	1.15
7.50	1.58
10.00	1.96
12.50	2.26
15.00	2.44
17.50	2.50
55.06	2.50

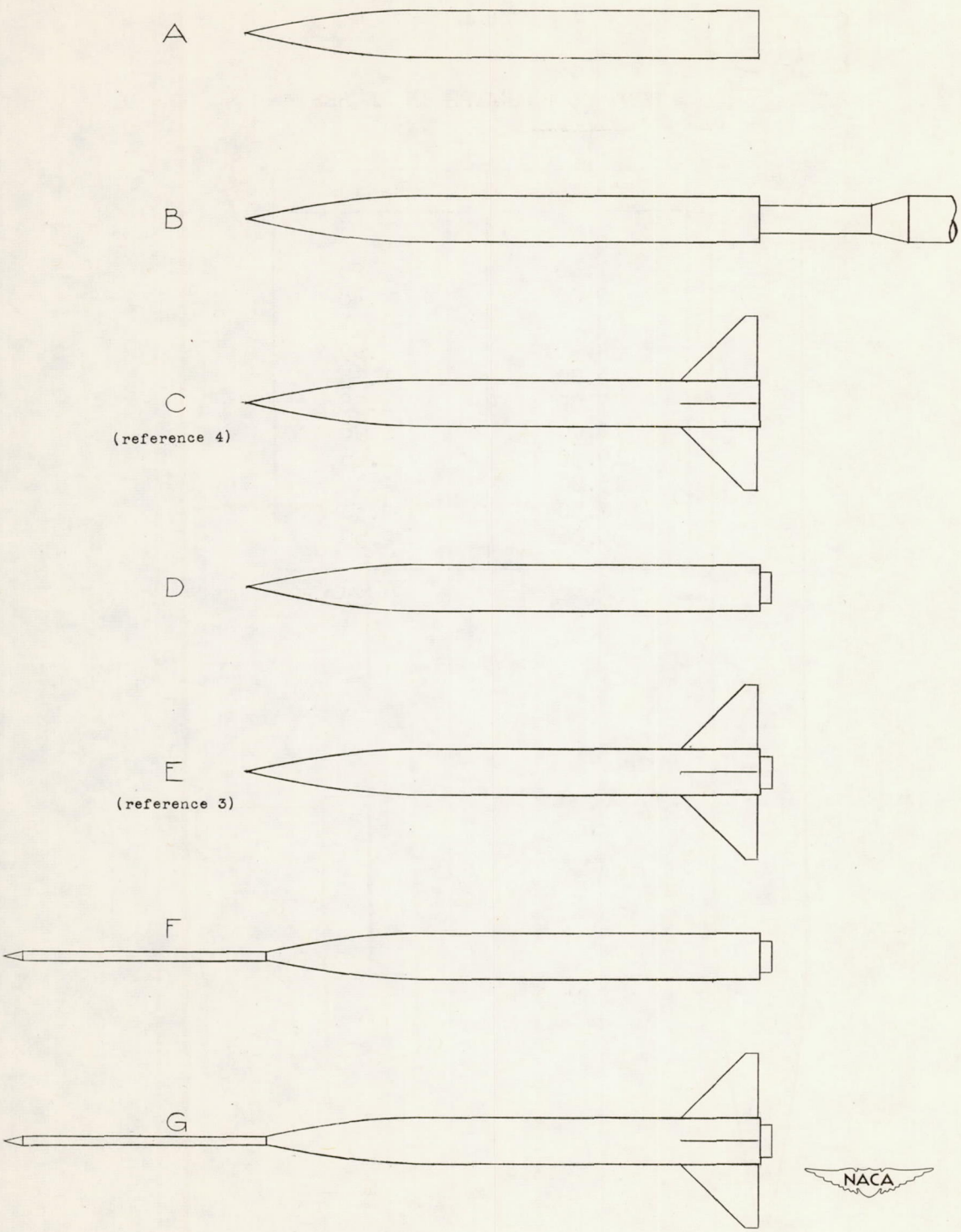

(a) General view.

Figure 1.- The test configurations. Dimensions are in inches.

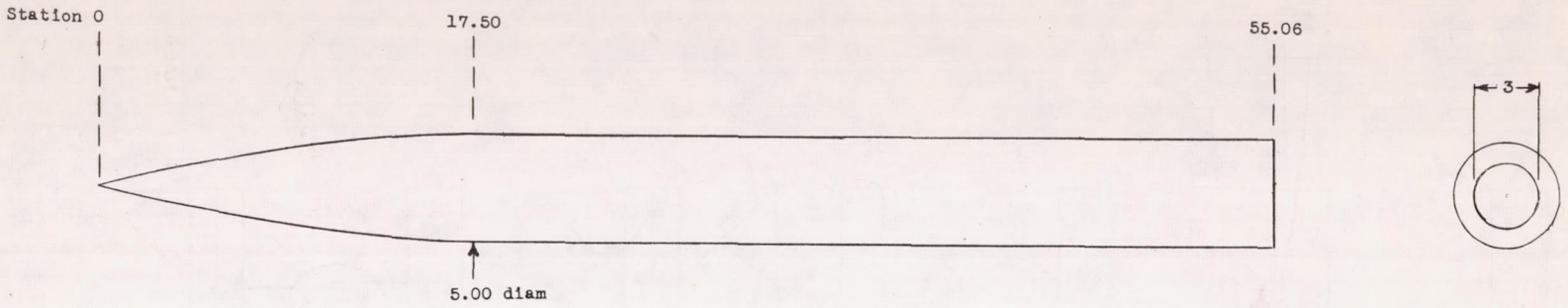

(b) Basic body.

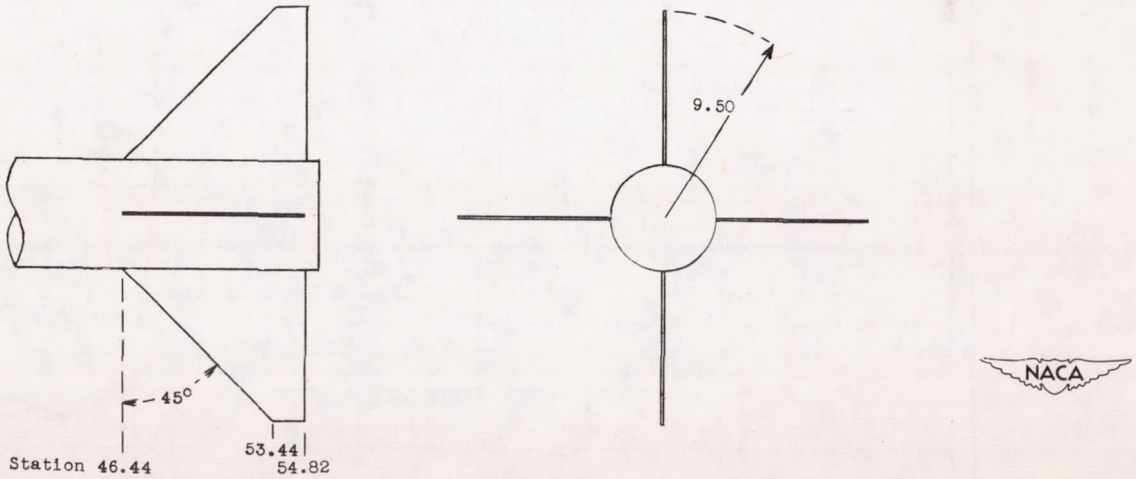

(c) Stabilizing fins.

Figure 1.- Continued.

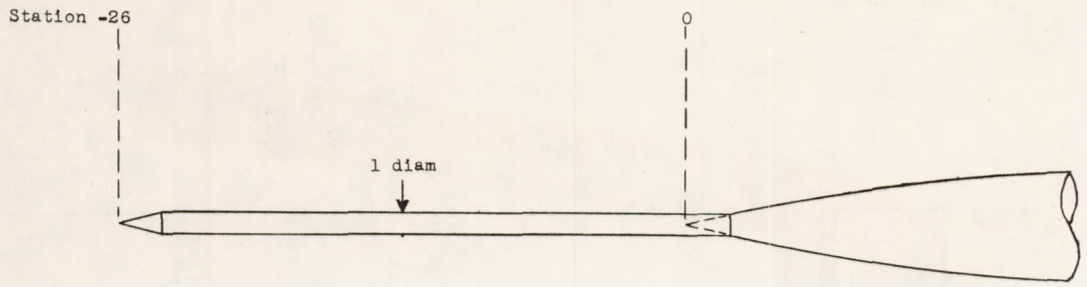

(d) Nose sting.

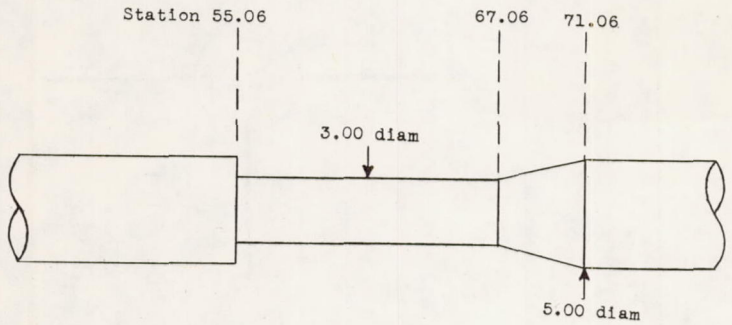

(e) Rear-support sting.

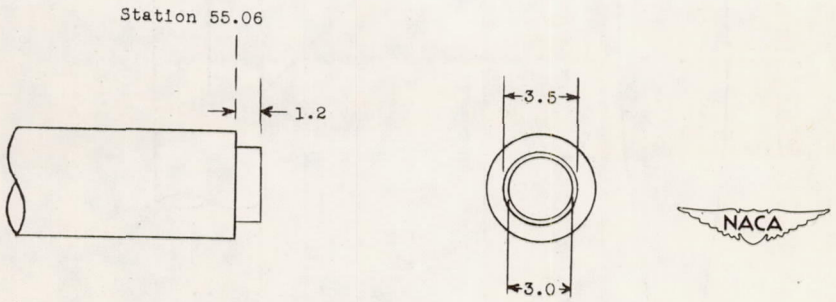

(f) Rocket tail nut.

Figure 1.- Concluded.

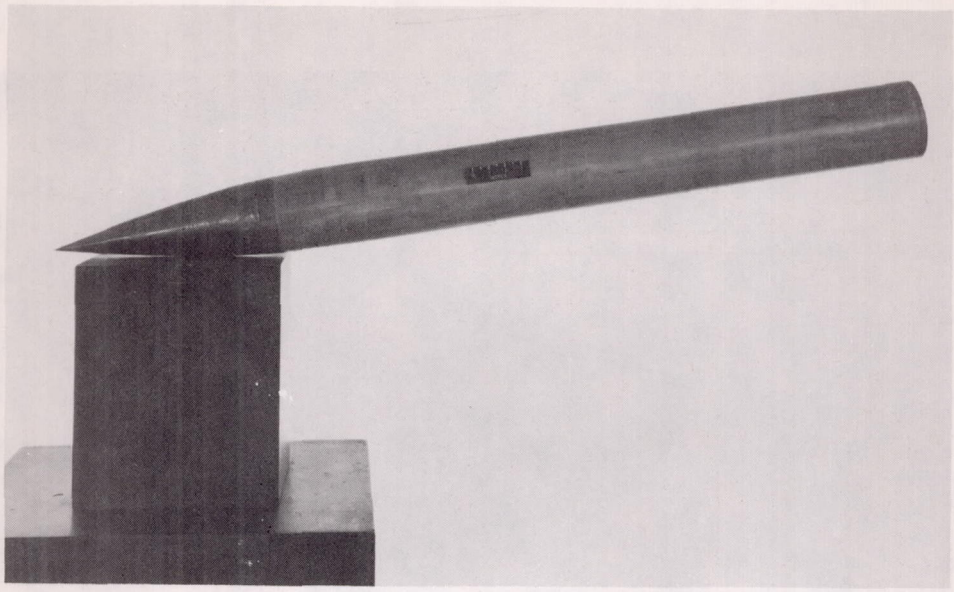

NACA

L-70351.1

Figure 2.- Base-pressure model, illustrating the center-of-gravity location.

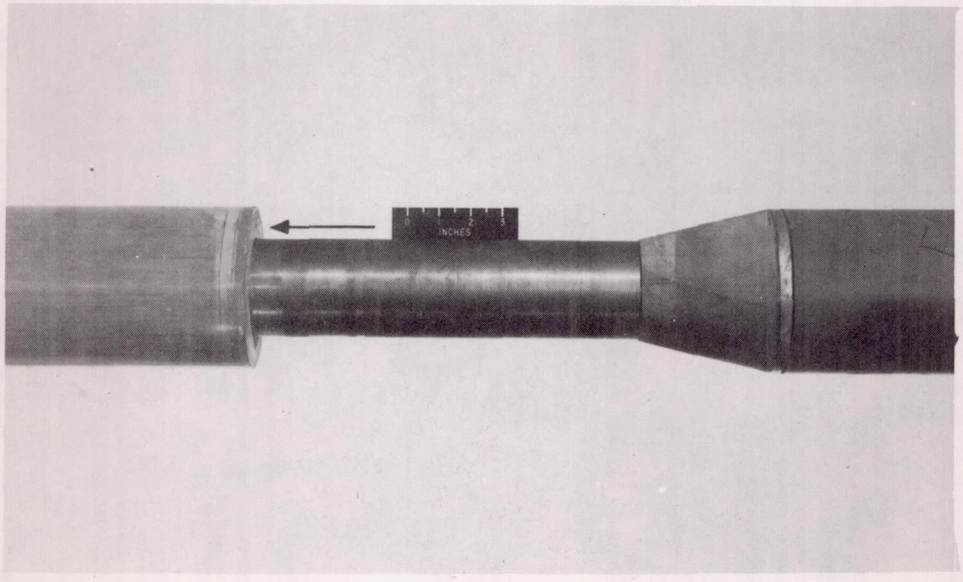

Figure 3.- Base-pressure model with booster, showing rim orifice location (arrow) and simulated wind-tunnel support.

NACA

L-70352.1

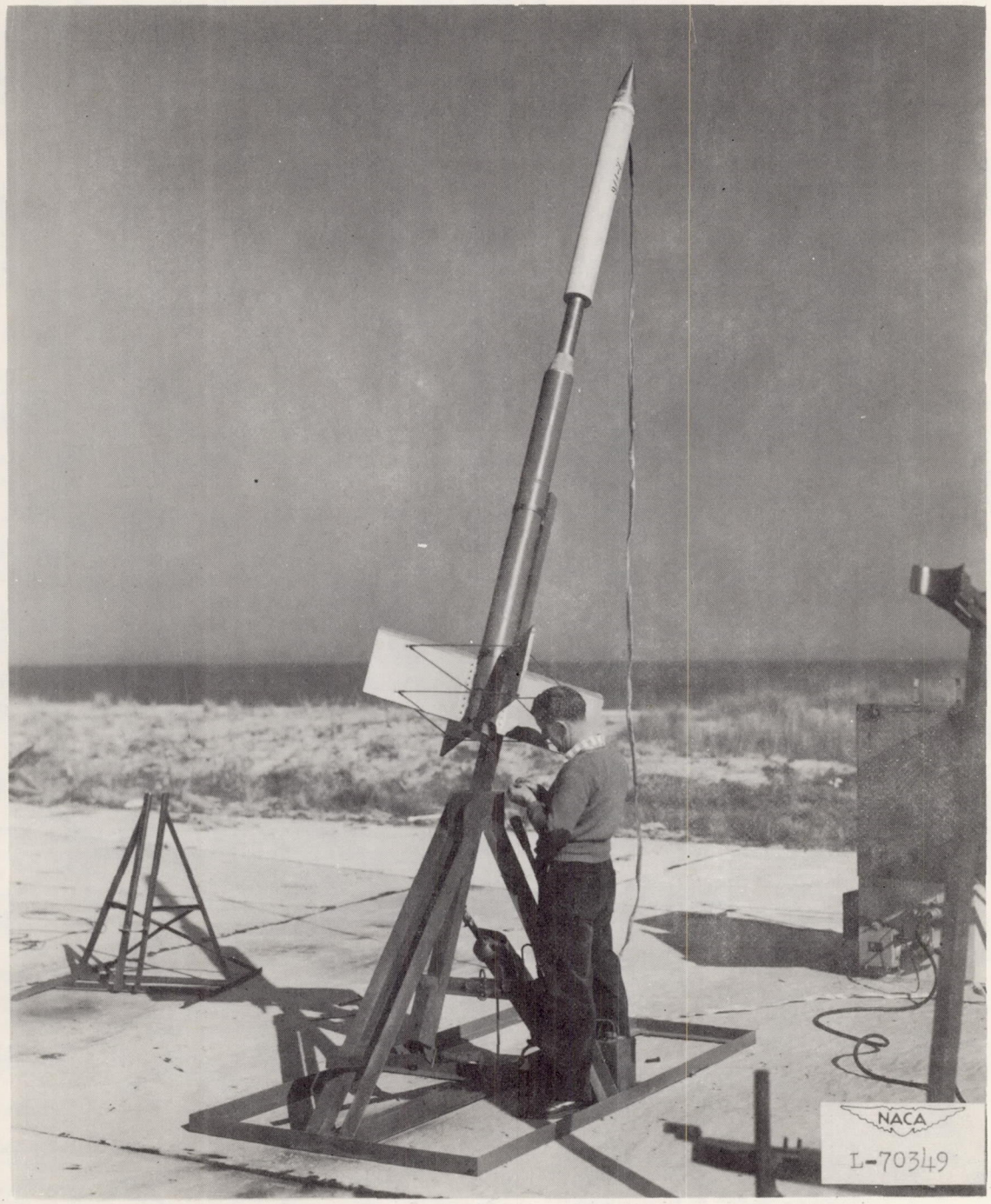

Figure 4.- Base-pressure model with booster on launcher.

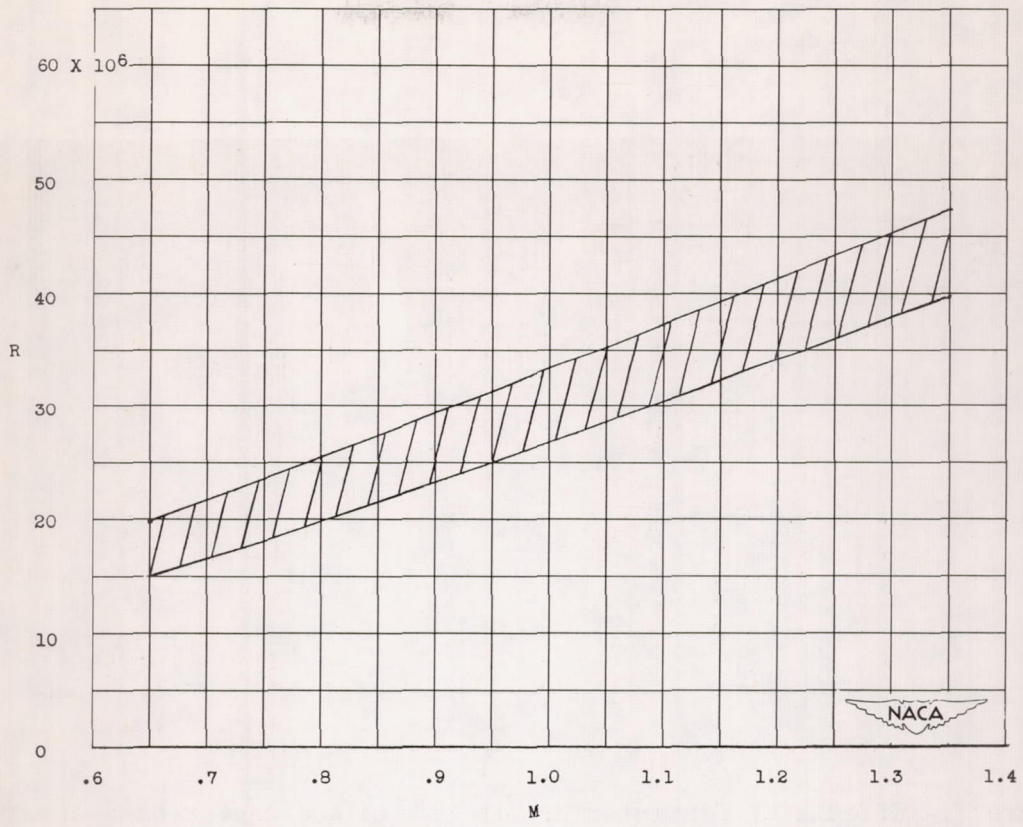

Figure 5.- Mach number - Reynolds number region of the flight tests.

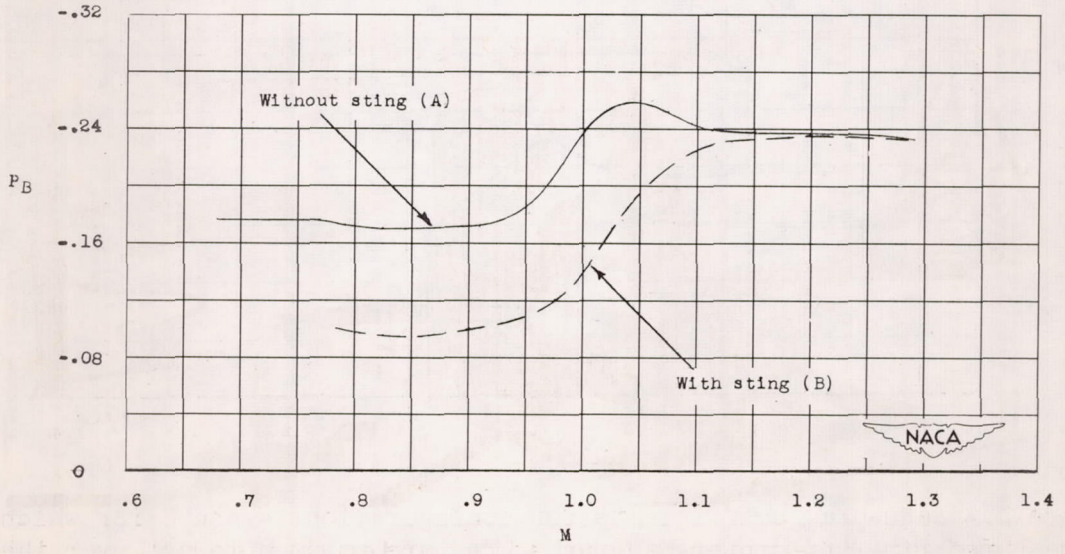

Figure 6.- Effects of the rear-support sting on rim-base-pressure coefficients.

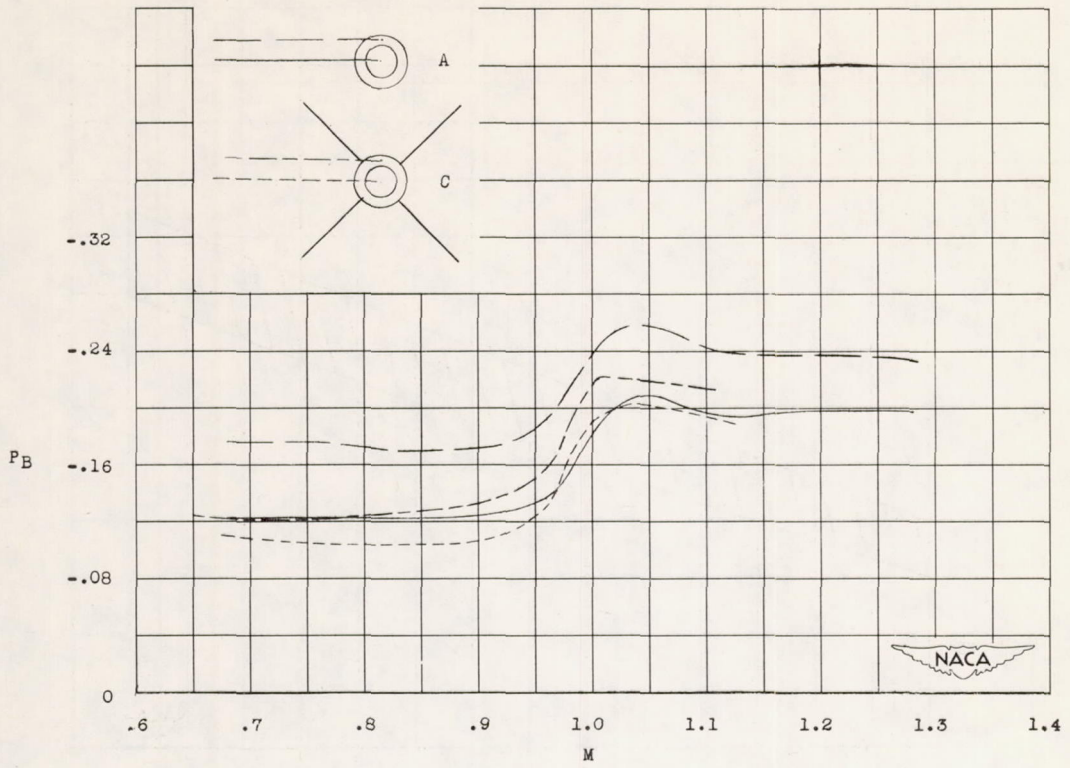

Figure 7.- Effects of fin interference on rim and center-base-pressure coefficients.

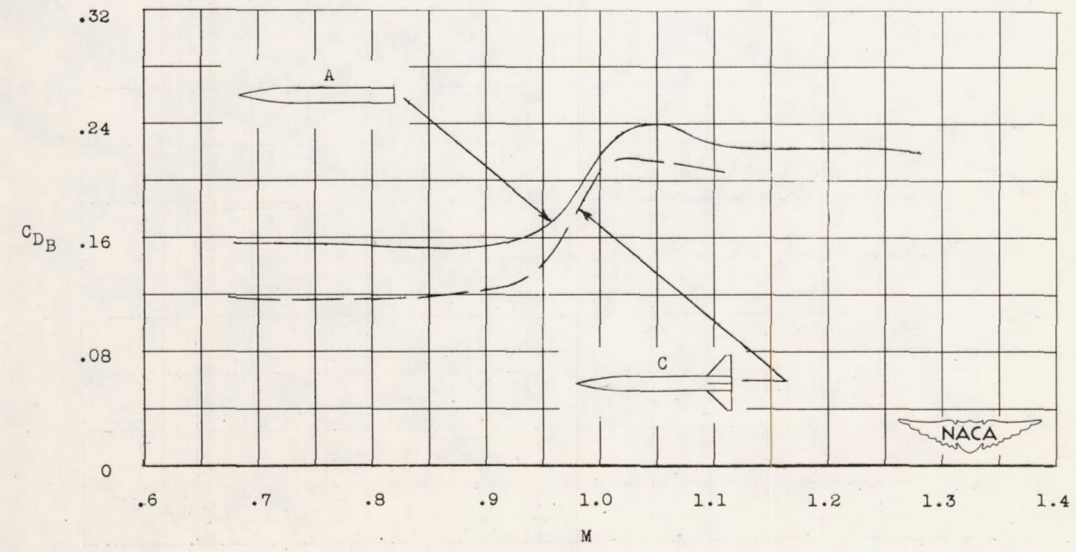

Figure 8.- Base-drag coefficients for configurations A and C for which measured rim- and center-base pressures are assumed to act over the entire respective areas.

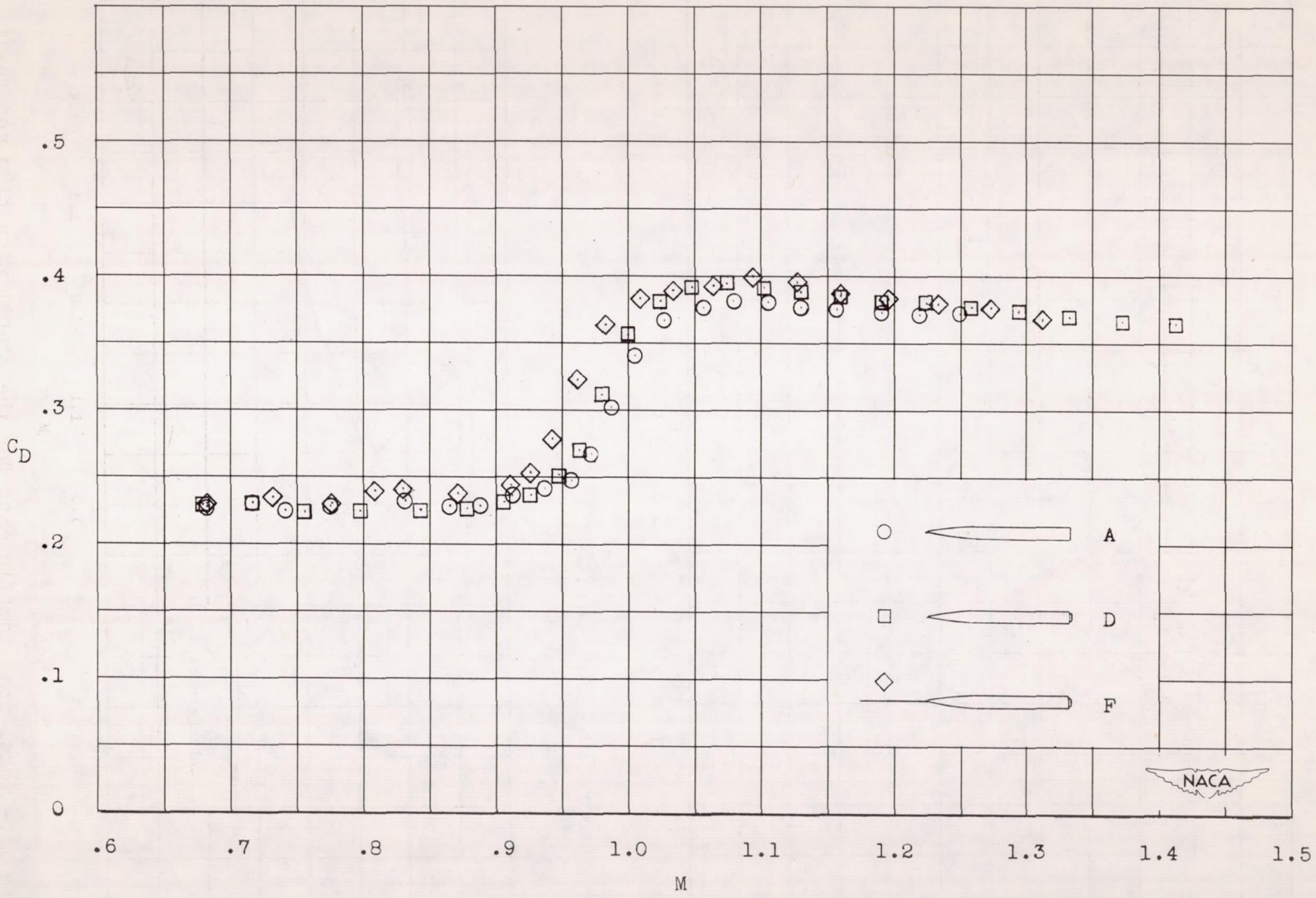

Figure 9.- Drag data for the wingless, finless fuselages.

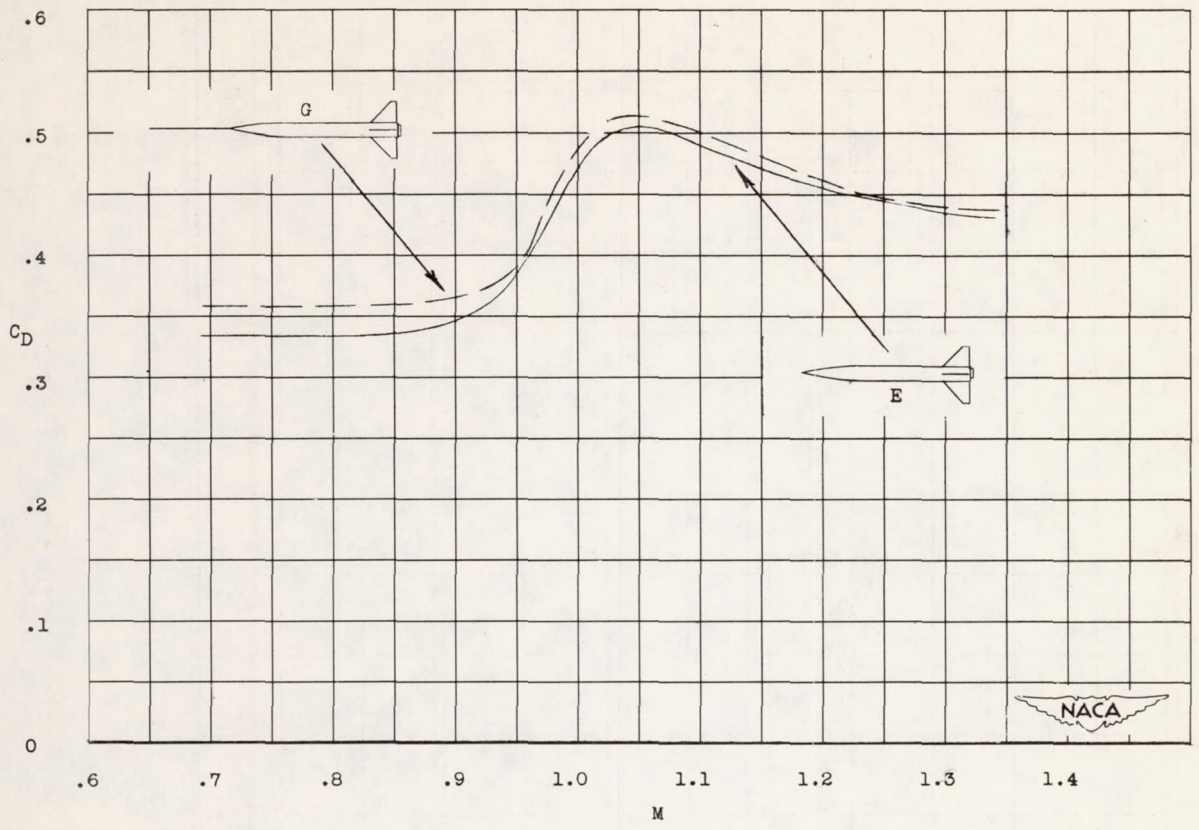

Figure 10.- Drag data for the fin-stabilized bodies.

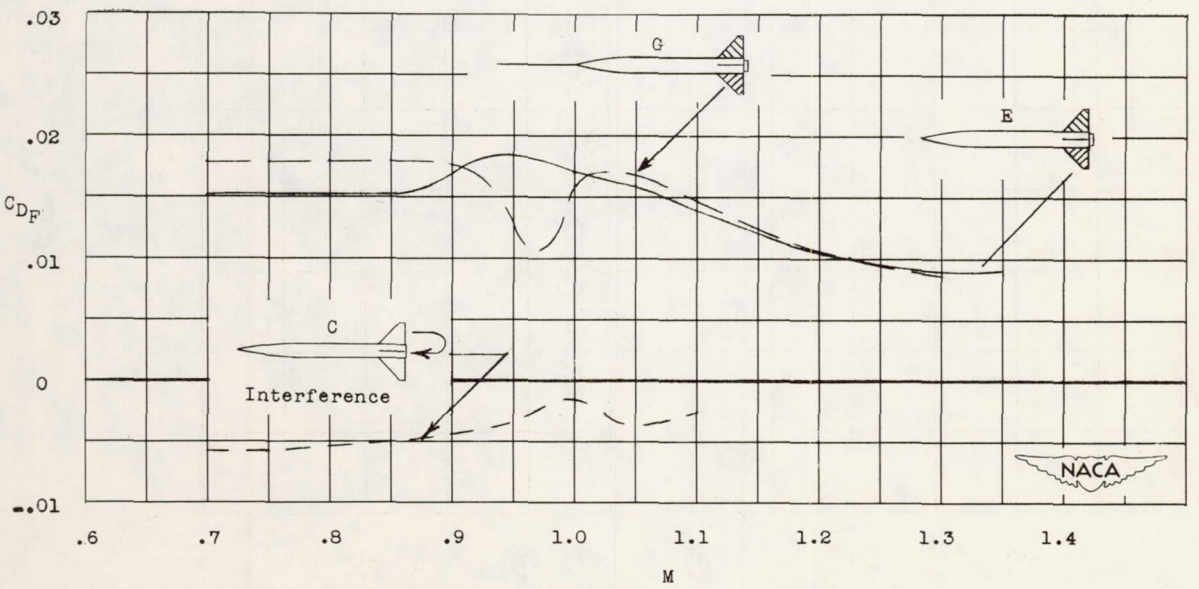

Figure 11.- Total-drag coefficients for the stabilizing fins and their effect on body base drag.

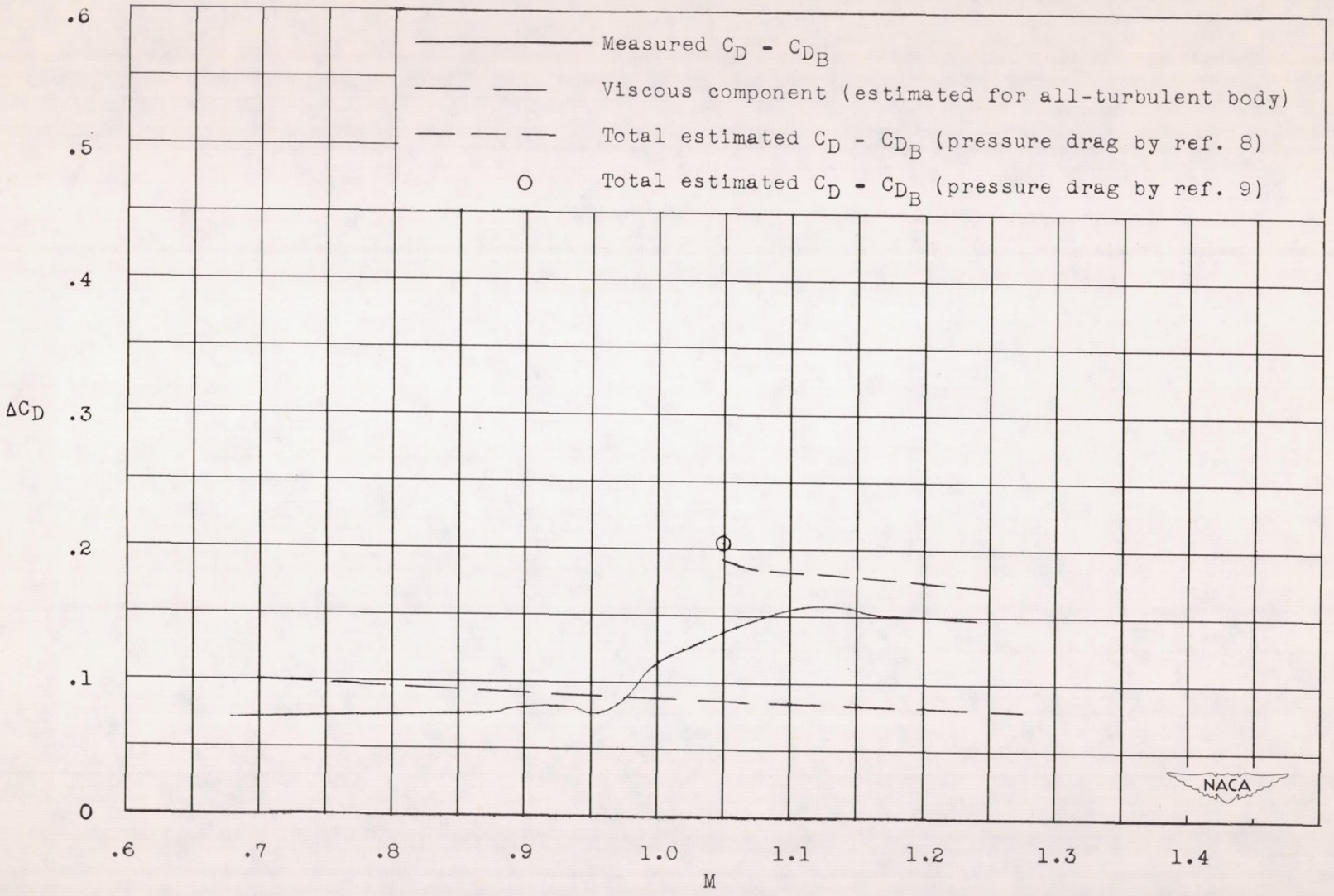

Figure 12.- Coefficients of fore drag and its estimated components for configuration A.